Research Paper

The Indian Ocean Dipole response to external forcing in the coupled model intercomparison project phase 5 simulations of the last millennium

Thanh Le[1,2] (iD) and Deg-Hyo Bae[1,2]

Abstract

The Indian Ocean Dipole (IOD) is a major mode of interannual climate variability, but its response to external climate forcings (i.e. solar forcing, volcanic radiative forcing (VRF) and greenhouse gas (GHG) radiative forcing) remains elusive. To improve our understanding of the variability of the IOD, it is necessary to investigate the IOD's response to external forcings through multi-model simulations. Here a Granger causality test is used to examine the impact of external forcings on the IOD from past 1000 years simulations (850–1850 Common Era) derived from Coupled Model Intercomparison Project Phase 5 (CMIP5) models. The results show significant causal effects of VRF on the IOD in preindustrial times of the past 1000 years from the MPI-ESM-P, MRI-CGCM3, GISS-E2-R and CCSM4 models and uncertainties in the IOD's responses to volcanic eruptions from other six models. Additionally, the phase responses (i.e. positive or negative) of the IOD to large volcanic eruptions remain unclear even from models showing significant causal impacts of VRF on the IOD. This result shows that the IOD exhibits a more complex response to volcanic forcing than the El Niño-Southern Oscillation. The causal impact of solar forcing on the IOD is more likely to be weak in most models. The IOD's response to GHG variations is not significant across all the models due to minor fluctuations in GHGs occurring during preindustrial times of the past 1000 years. Further analyses based on new, improved and higher resolution models might further our understanding of the IOD's responses to external forcing.

Introduction

The global climate is influenced by several major climate drivers, including the Indian Ocean Dipole (IOD; Saji et al., 1999; Webster et al., 1999). The IOD is the main climate mode that generates extreme climatic patterns in the Indian Ocean (IO) and in surrounding regions. The positive phase of the IOD is characterized by warmer than normal sea surface temperatures (SSTs) in the western tropical IO and by cooler temperatures to the east (Saji et al., 1999; Webster et al., 1999). Severe effects of the IOD include the formation of droughts in Australia (Ashok et al., 2003; Cai et al., 2009; Ummenhofer et al., 2009), East Asia (Kripalani et al., 2009), and western Indonesia (Abram et al., 2003) and the generation of heavy rains in East Africa (Behera et al., 2006; Black et al., 2003). While there may be similarities between past and present day IOD events (Tangunan et al., 2017), understanding the IOD's responses to external forcings (i.e. solar forcing, volcanic radiative forcing (VRF) and greenhouse gas (GHG) radiative forcing) is critical to forming predictions of future climate extremes observed in and around the IO (Cai et al., 2014; Lazenby et al., 2018).

Volcanic activity influences the climate system by reducing incoming solar insolation at the Earth's surface, resulting in global surface cooling (e.g. Robock, 2000). Solar forcing was an important natural factor that shaped climate change in preindustrial times of the past 1000 years (e.g. Solanki et al., 2013), and it has a significant impact on surface air temperatures in areas of the

tropics and subtropics, including the IO (Le, 2015; Le et al., 2016; Zambri et al., 2017). Although there uncertainties and discrepancies remain regarding the magnitude of solar effect on global climatic patterns (e.g. Schurer et al., 2013), solar forcing may impact IOD variations. Changes in concentrations of long-lived GHGs (e.g. CH_4, CO_2, and N_2O) lead to variations in radiative forcing (or to the modulation of the radiative energy budget of the Earth's climate system (Ramaswamy et al., 2001)) by absorbing longwave radiation in the troposphere, resulting in climate change.

Most studies related to the influence of external forcings on tropical climates focus on the connection between these factors and the El Niño-Southern Oscillation (ENSO; Khodri et al., 2017; Le, 2017; Zuo et al., 2018) while the relationship between these

[1]Department of Civil & Environmental Engineering, Sejong University, Seoul, South Korea
[2]Center for Climate Change Adaptation for Water Resources, Sejong University, Seoul, South Korea

Corresponding authors:
Thanh Le, Department of Civil & Environmental Engineering, Sejong University, 05006, 209 Neungdong-ro, Gwangjin-gu, Seoul, South Korea.
Deg-Hyo Bae, Department of Civil & Environmental Engineering, Sejong University, 05006, 209 Neungdong-ro, Gwangjin-gu, Seoul, South Korea.
Emails: levinhthanh.lvt@gmail.com; dhbae@sejong.ac.kr

forcings and the IOD remains elusive. Few efforts (e.g. Izumo et al., 2018; Maher et al., 2015; Zheng et al., 2013) have been made to quantify the IOD responses to external forcings. Studies have used select model and CMIP5 historical simulations (i.e. 1850–2005) to show that volcanic forcing increases the likelihood of a positive IOD emerging from eruptions of the following year (Maher et al., 2015) while tropical volcanic eruptions create a subsurface ocean response similar to a negative IOD in the year of an eruption (Izumo et al., 2018). Increase in concentrations GHGs induces an IOD-like warming pattern in the tropical Indian Ocean but does not alter the interannual variance of the IOD (Zheng et al., 2013).

In this study, we investigate the causal connection between external forcings and the IOD of the past 1000 years via model simulations based on multivariate vector autoregressive time series models and Granger causality tests (see Methods Section 2). Our method considers the simultaneous impacts of different factors (i.e. VRF, solar forcing, and GHG radiative forcing), and thus it may present more robust results of the IOD responses to these forcings. Specifically, in this study we quantify the probability of the IOD responding to external forcings. From long-term simulations for the past 1000 years with large multi-model results, the results of this study may improve the statistical significance of the true link between external forcings and the IOD. The results of this study may also serve as an evaluation of climate models' levels of consistency in simulating IOD responses to external forcings.
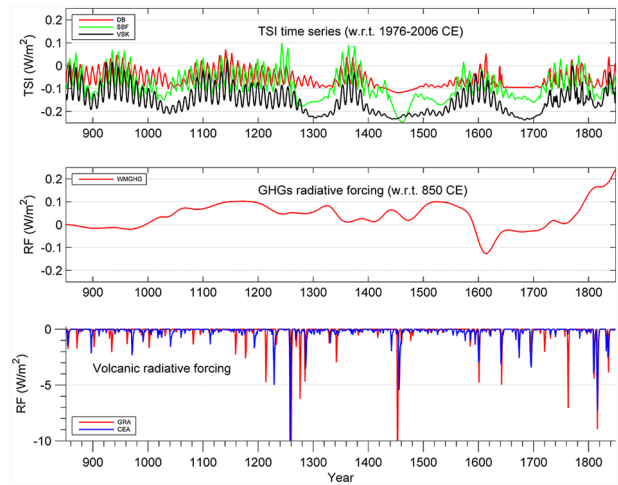
Data

Monthly mean SST and near-surface eastward wind data are taken from the Coupled Model Intercomparison Project Phase 5 (CMIP5) model simulations for the past 1000 years (simulation name "past1000"; Taylor et al., 2012). The simulations roughly start in the 850 Common Era (CE) and roughly end in 1850 CE. Thus, in this study, the last millennium refers to the 850–1850 CE period.

The models were forced with Total Solar Irradiance reconstructions taken from Vieira et al. (2011), Delaygue and Bard (2010), Steinhilber et al. (2009) or Wang et al. (2005) (see Supplemental Table S1). In Supplemental Table S1, volcanic forcings used in each simulation were drawn from Crowley et al. (2008) or Gao et al. (2008). Figure 1 shows the time series for these climate forcings. Other sources of forcing include well-mixed greenhouse gas (GHG) variations. Further information on climate forcing reconstruction selections employed in CMIP5 in simulations for the past 1000 years are described in Schmidt et al. (2011, 2012).
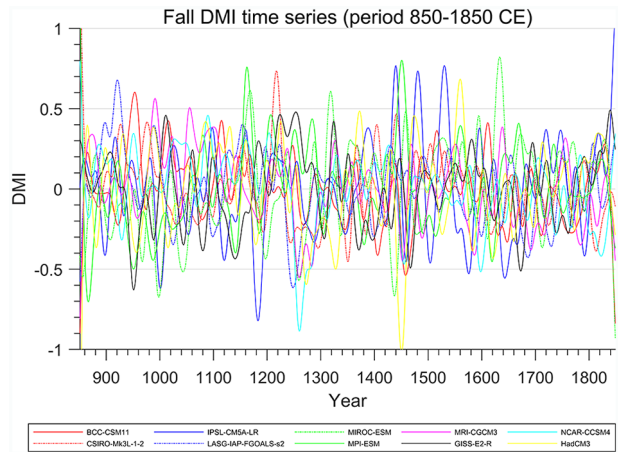
The simulation of the IOD in CMIP5 models is crucial and is discussed in previous studies. For example, several CMIP5 models may not capture the IOD's spatial structure mainly for equatorial regions of the Indian Ocean (Chu et al., 2014), and the IOD's amplitude can be overestimated (Weller and Cai, 2013). Besides, several models underestimate the temperature change between the Little Ice Age (i.e. 1450–1850 CE) and the Medieval Climate Anomaly (i.e. 950–1250 CE) for most parts of the Northern Hemisphere (Ljungqvist et al., 2019). Although CMIP5 models might exhibit biases in simulating IOD variations, these models provide useful datasets for understanding IOD responses to external forcings.

Methods

The dipole mode index (DMI; Saji et al., 1999) is defined as the difference in boreal autumn (September-October-November, SON) SST anomalies observed between the tropical western IO (50°E–70°E; 10°N–10°S) and the tropical south-eastern IO (90°E–110°E; 0°N–10°S). Changes in the DMI of the past 1000 years are highly model dependent (see Figure 2 for filtered

Figure 1. Solar forcing, GHG radiative forcing and volcanic forcing for 850–1850 CE (see Supplemental Table S1 for climate forcing reconstruction options used in past 1000-year CMIP5 simulations). Solar forcing (from DB, VSK, and SBF) is shown as TSI with respect to the (w. r. t.) mean TSI for 1976–2006. GHG radiative forcing is shown as w. r. t. radiative forcing (RF) for the year 850. Volcanic forcing spurs negative radiative forcing within the climate system. GHGs: greenhouse gases; TSI: Total Solar Irradiance.

Figure 2. The dipole mode index (DMI) is defined as the difference between boreal autumn (September-October-November, SON) SST anomalies and those of the tropical western Indian Ocean (50°E–70°E; 10°N–10°S) and tropical southeastern Indian Ocean (90°E–110°E; 0°N–10°S). The DMI is shown for individual models. Time series are shown as 15-year low-pass-filtered data (for visualization only).
SST: sea surface temperature.

DMI time series of individual models). Nevertheless, there is consistency in simulating the range of DMI amplitudes between models except in the case of the minor wide spread of DMI amplitudes given in model IPSL-CM5A-LR (solid blue line).

Multivariate vector autoregressive (VAR) time series models (e.g. Mosedale et al., 2006) are employed to evaluate the impact of external forcings (i.e. solar forcing, volcanic forcing and GHGs radiative forcing) on the DMI. This method employs the following definition of Granger causality (Granger, 1969): variable Y has a causal influence on variable X when information given by past values of Y is helpful in facilitating the prediction of X. The pth order vector autoregressive VAR(p) is defined as:

$$X_t = \sum_{i=1}^{p} \alpha_i X_{t-i} + \sum_{i=1}^{p} \beta_i Y_{t-i} + \sum_{j=1}^{m} \sum_{i=1}^{p} \delta_{j,i} Z_{j,t-i} + \varepsilon_t \quad (1)$$

where X_t is the DMI for year t, Y_t is the considered forcing for year t, $Z_{j,t}$ is the control forcing j for year t, m is total number of control forcings, and $p \geqslant 1$ is the ordering of the causal model. We define either volcanic radiative forcing (VRF) or Total Solar Irradiance (TSI) or GHG radiative forcing as considered forcing. Other forcings are defined as control forcings (or defined as the confounding factors (Hegerl et al., 2010) or control variables (Stern and Kaufmann, 2013). For example, when VRF is considered forcing, TSI and GHG radiative forcing are control forcings. Control forcings may affect the relationship between the considered forcing and the DMI. In equation (1), m is equal to 2, and hence we consider two forms of control forcing in our analyses. Terms α_i, β_i, and $\delta_{j,i}$ are regression coefficients, and ε_t is the noise residual in the regression. These regression coefficients and residuals are computed using the least squares method of the multiple linear regression analysis approach. The data time series of X, Y, and $Z_{1 \to m}$ are normalized and detrended. Whether detrending is applied or not does not alter our overall conclusions.

A Granger causality test is applied to the causal model described in equation 1. In applying this test, the probability of no Granger causality being present is used to evaluate the causal relationship between X and Y. The predictive model described in equation (1) is considered as a complete model where all variables (i.e. external climate forcings and past data of DMI) are employed to estimate DMI. The null model of no causal impacts from a given climate forcing (i.e. variable Y) to DMI is established by removing the terms related to Y in equation (1) (i.e. by setting). The null model and the complete model are then differentiated by using the following indicator:
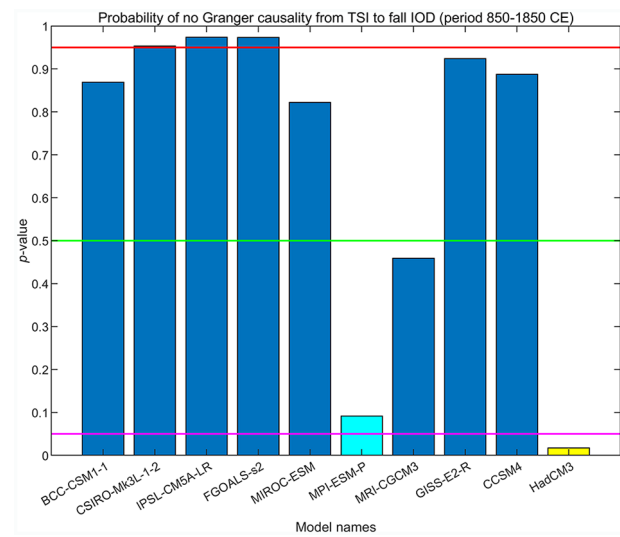
$$L_{Y \to X} = n(\log|\Omega_{p,\beta_i=0}| - \log|\Omega_p|)$$

where $|\Omega_p|$ is the determinant of the covariance matrix of the noise residual, and n is the length of the data time series. We assess the significance of the complete predictive model by matching the computed $L_{Y \to X}$ indicator against a null distribution. This assessment results in a probability for no causal influence of the considered climate forcing (i.e. variable Y) on DMI. Further information on this test is given in previous works (Le et al., 2016; Mosedale et al., 2006). The methods presented in this study are designed to detect causal effects and thus, provide robust evaluation of possible impacts of external climate forcing on the IOD. The results are also supported by the multi-model approach.

The predictive model described in equation (1) may contain uncertainties if the effects of an important forcing (e.g. ENSO which is normally considered as the strongest climate mode of interannual climate variability) of the IOD are neglected (Lütkepohl, 1982). Thus, we will discuss the role of ENSO on the causal influences of external forcing on the IOD.

Results and discussion

Figure 3 shows the probability of there being no Granger causality between solar forcing and the IOD of individual models. This result demonstrates that solar activity is only found to have significant causal influence on IOD variations in the HadCM3 (at the 5% significance level) and MPI-ESM-P models (at the 10% significance level). In Figure 3, 7 out of 10 models show p-values exceeding 50%, indicating that a weak IOD response to TSI is favored in the models. This result suggests that IOD events may not be triggered by solar forcing. Although several studies (e.g. Le, 2015; Le et al., 2016; Meehl et al., 2008) indicate that solar variations may influence tropical Indian Ocean (IO) near surface air temperatures, the non-significant response of the IOD to solar forcing suggests that other forcings and internal variability have played a more important role in inducing IOD variations over the past 1000 years. Our result is partly in agreement with previous studies (Schurer et al., 2013) showing minor effects of solar

Figure 3. Probability of an absence of Granger causality from TSI to the DMI. Probability (p-value) values are shown for individual models. Horizontal red, green and magenta lines mark p-values of 0.95, 0.5, and 0.05, respectively. Models with p-values exceeding 0.05 fail to reject the null hypothesis of there being no Granger causality between TSI and the DMI at the 5% significance level. The results of models MPI-ESM-P (p-value < 0.1) and HadCM3 (p-value < 0.05) are plotted as cyan and yellow bars, respectively.
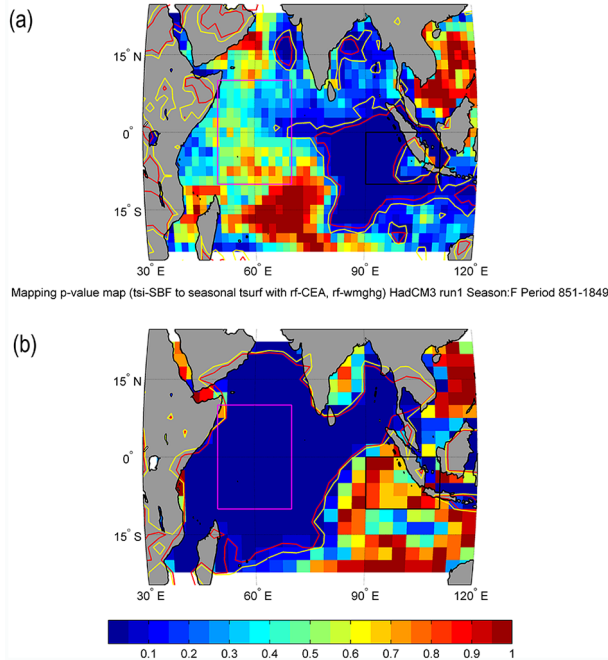TSI: Total Solar Irradiance; DMI: dipole mode index.

forcing on the climate of Northern Hemisphere over past millennium.

Figure 4a shows significant SST response to TSI in part of eastern IO during boreal autumn for model MPI-ESM-P while the response in the western IO is weaker. Figure 4b shows a significant level of Granger causality between TSI and the western IO SST for the boreal autumn season for model HadCM3 and a weak connection between TSI and the boreal autumn SST of the eastern IO. In eastern parts of the tropical and subtropical IO interactions occur between the IO and the tropical Pacific, which are normally controlled by internal climate variability (e.g. air-sea interactions in tropical areas of the Indian and Pacific Oceans or the modulation of zonal winds that may affect SST variations (Cai et al., 2019; Latif and Barnett, 1994; Sprintall et al., 2014; Tokinaga et al., 2012)). This result indicates that even for models showing significant Granger causal impacts of TSI to the DMI, solar forcing still might not entirely influence the tropical and subtropical IO SST. This weak control of solar forcing on tropical and subtropical IO SSTs may be associated with the IOD's non-significant response to solar forcing shown in most models.

Figure 5 shows non-significant causal effects of GHG variations on the DMI. This result indicates that GHG variations may not have had a major influence on regional climate changes in tropical and subtropical areas of the IO over the past 1000 years. This result may not be surprising due to minor fluctuations in GHGs occurring the during preindustrial period of the last millennium. Impacts of GHG variations on the DMI may have changed in the industrial period (i.e. 1850 to the present) and may change in the future (Cai et al., 2013) with stronger fluctuations in GHGs. As no model shows significant influences of GHGs variations on the DMI, we did not further investigate the impacts of GHG variations on IO SSTs.
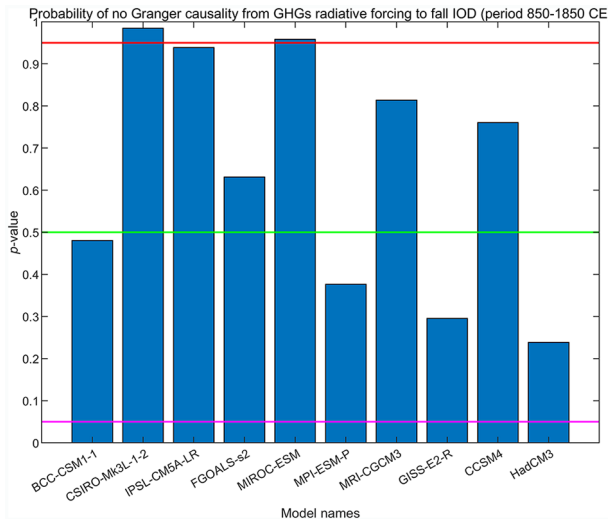
Figure 6 shows that the IOD is more sensitive to VRF in some models than others. Specifically, four models (MPI-ESM-P, MRI-CGCM3, GISS-E2-R, and CCSM4) show significant Granger causality for VRF's effect on the IOD. This inconsistency may be attributed to discrepancies between models concerning oceanic responses recorded after volcanic eruptions (Ding and Carton, 2014; Mignot et al., 2011). In addition, IOD responses shown in

Mapping p-value map (tsi-SBF to seasonal tsurf with rf-CEA, rf-wmghg) MPIESMP run1 Season:F Period 851-1849

Mapping p-value map (tsi-SBF to seasonal tsurf with rf-CEA, rf-wmghg) HadCM3 run1 Season:F Period 851-1849

Figure 4. Probability of an absence of Granger causality from TSI to tropical and subtropical Indian Ocean boreal autumn (September-October-November) SSTs according to models MPI-ESM-P (a) and HadCM3 (b). The red (yellow) contour line shows that the p-value = 0.05 (0.1). Red shades mark a high probability of an absence of Granger causality. Magenta and black boxes indicate tropical western Indian Ocean (50°E–70°E; 10°N–10°S) and the tropical south-eastern Indian Ocean (90°E–110°E; 0°N–10°S), respectively.
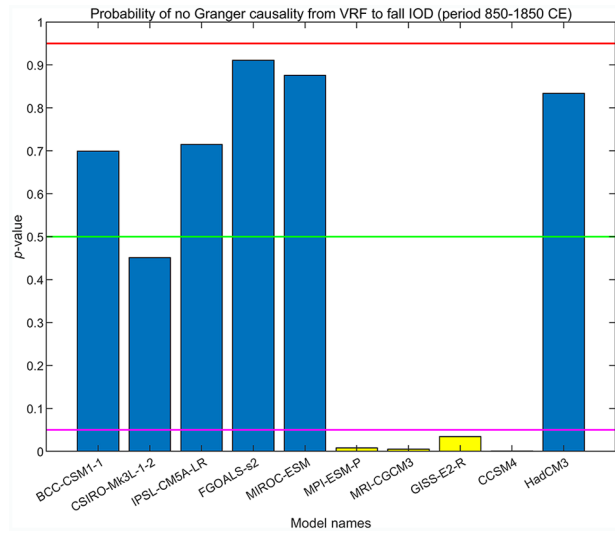TSI: Total Solar Irradiance; SST: sea surface temperature.

Figure 5. The same data given in Figure 3 but for a Granger causality from well-mixed greenhouse gas radiative forcing to the DMI.
DMI: dipole mode index.

the models are not robust (Swingedouw et al., 2017) and several models simulated weak internal variability and feedback mechanisms (Gómez-Navarro et al., 2015; Ljungqvist et al., 2019). Other studies suggest that climatic responses (e.g. oceanic evolution) to strong volcanic eruptions vary in CMIP5 climate models and the causes of the spread between models are related to the VRF employed in each model, the background climate and

Figure 6. The same data given in Figure 3 but for a Granger causality from volcanic radiative forcing (VRF) to the DMI. The four models (results are plotted as yellow bars) show the Granger causality between VRF and the DMI at the 5% significance level. See Supporting Supplemental Figure S1 for the DMI's responses to VRF at different latitudes.
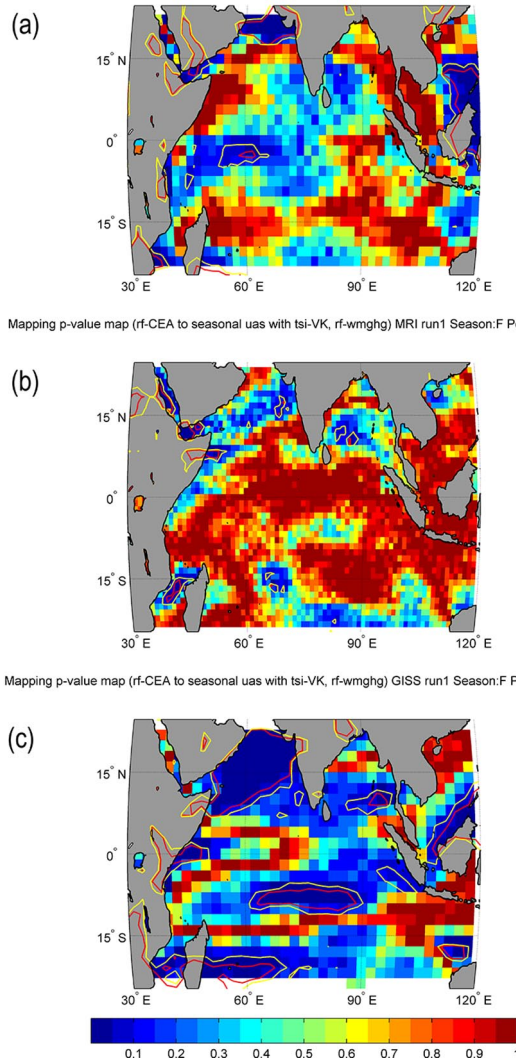DMI: dipole mode index.

internal climate variability (e.g. Zanchettin et al., 2016). IOD responses to VRF at different latitude bands are shown in Supplemental Figure S1. We note that IOD responses to VRF at low latitudes (i.e. the 0°S–30°S and 0°N–30°N bands) are more significant than those observed at high latitudes (i.e. the 30°S–90°S and 30°N–90°N bands) in several models (i.e. CSIRO-Mk3L-1-2, GISS-E2-R).

A further analysis reveals a significant causal influence of volcanic forcing on tropical and subtropical IO autumn SST (Supplemental Figure S2) according to the MPI-ESM-P, MRI-CGCM3, GISS-E2-R, and CCSM4 models. These models reveal a Granger causal connection between VRF and SST for a large proportion of the tropical and subtropical IO. This result suggests that surface basin cooling effects observed after volcanic eruptions might occur simultaneously in tropical and subtropical areas of the IO and may thus directly shape effects of VRF on the IOD.

The tropical Pacific contributes to the evolution of the tropical Indian Ocean and the IOD (Cai et al., 2019). This effect is exerted via the oceanic pathway through the Indonesian Archipelago (Sprintall et al., 2014), or via the changes in Walker circulation induced by ENSO (Latif and Barnett, 1994). The mechanisms for the connection between the Pacific and Indian Oceans are difficult to model correctly, as they require accurate parameterization of atmospheric convection over the tropics and a realistic representation of the Indonesian Throughflow. One may assume that volcanic eruptions have effects on ENSO [computed as the average SST anomalies in the Niño 3.4 area (120–170°W; 5°N–5°S) in boreal winter (December–January–February)], then the modified ENSO signal would likely affect the IOD. Additional analysis reveals that the effects of VRF on IOD slightly decrease for models GISS-E2-R and MRI-CGCM3 when ENSO is included to the predictive model described in equation (1) as a confounding factor (Supplemental Figure S3). However, three models (MPI-ESM-P, MRI-CGCM3, and CCSM4) still show significant Granger causality for VRF's effect on the IOD. Thus, the overall response of the IOD to VRF is significant, but this response is partly dependent on the representation of ENSO in the models.

Figure 7 shows a probability map for an absence of Granger causality between VRF and boreal autumn surface eastward winds (i.e. surface zonal winds) for the tropical and subtropical
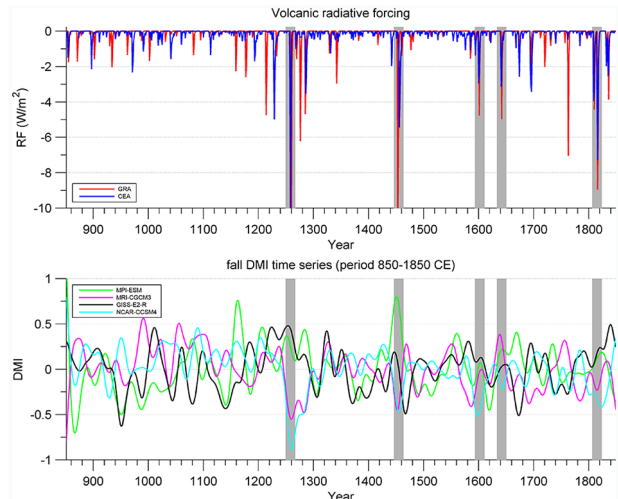
Mapping p-value map (rf-CEA to seasonal uas with tsi-VK, rf-wmghg) MPI run1 Season:F Period 851-1849

(a)

Mapping p-value map (rf-CEA to seasonal uas with tsi-VK, rf-wmghg) MRI run1 Season:F Period 851-1849

(b)

Mapping p-value map (rf-CEA to seasonal uas with tsi-VK, rf-wmghg) GISS run1 Season:F Period 851-1849

(c)

0.1 0.2 0.3 0.4 0.5 0.6 0.7 0.8 0.9 1

Figure 7. Probability of an absence of a Granger causality from VRF to the tropical and subtropical Indian Ocean boreal autumn (September–October–November) surface eastward winds according to the models MPI-ESM-P, MRI-CGCM3, and GISS-E2-R, respectively. The red (yellow) contour line shows that the *p*-value = 0.05 (0.1). Red shades mark a high probability of an absence of Granger causality.
VRF: volcanic radiative forcing.

Figure 8. Phase (i.e. positive or negative) response of the DMI to large volcanic eruptions over the past 1000 years according to the models MPI-ESM-P, MRI-CGCM3, GISS-E2-R, and CCSM4. The upper figure shows variations in volcanic forcing for 850–1850 CE. The lower figure shows variations in the DMI. The grey bars denote periods when large volcanic eruptions occurred. The phase response of the DMI is positive for the models MPI-ESM-P and GISS-E2-R (green and black solid lines), while it is negative for the models MRI-CGCM3 and CCSM4 (magenta and cyan lines).
DMI: dipole mode index.

IO. The results are shown for models MPI-ESM-P, MRI-CGCM3, and GISS-E2-R where significant causal effects of VRF on the IOD are found. Surface eastward wind data for model CCSM4 were not available at the time of the study. In Figure 7, VRF is shown to have a causal influence on components of western IO surface zonal winds forming to the east of the African continent. The connection between VRF and IO surface zonal winds is weaker in the southeastern IO than in the northwestern IO, revealing the important impacts of internal climate variability on southeastern IO zonal wind variations. The results shown in Supplemental Figures S2 and 7 suggest that physical mechanisms related to changes in IO zonal winds occurring after volcanic eruptions might not play a significant role in the causal effects of VRF on IO SST and the IOD.

Figure 8 shows the response of the DMI to large volcanic eruptions and shows that periods in which large volcanic eruptions occur (denoted by grey bars) normally coincide with local maximum or minimum DMI values. Previous studies show that volcanic eruptions increase the likelihood of positive IOD events

occurring in the following year (Maher et al., 2015) and that tropical volcanic eruptions can induce a negative IOD in the year of an eruption (Izumo et al., 2018). However, Figure 8 shows that phase responses of the IOD following large volcanic eruptions remain unclear even from models showing significant connections between VRF and the DMI. For example, responses of the selected models to large volcanic eruptions occurring in the mid-13th century are not consistent. Specifically, models GISS-E2-R and MPI-ESM-P show positive DMI responses while models MRI-CGCM3 and CCSM4 present negative DMI responses. For other periods including large volcanic eruptions (as indicated by the grey bars in Figure 8), phase responses of the IOD also vary between the four models. Overall, for all five periods with strong VRF, the phase response of the IOD is positive according to models MPI-ESM-P and GISS-E2-R (both models use CEA data, see Supplemental Table S1) while it is negative according to models MRI-CGCM3 and CCSM4 (both models use GRA data). Thus, the IOD phase response to strong VRF might depend on the specific model used and on volcanic forcing data used in each model. This result is in agreement with the results of a recent study (Zanchettin et al., 2016). While periods involving large volcanic eruptions have been shown to coincide with periods of low ENSO indexes (Le, 2017), as is shown in Figure 8, periods of low DMI indexes occur independent of periods presenting high levels of volcanic forcing. Hence, the results given in Figure 8 also show that IOD responses to VRF are different and may be more complex than those of the ENSO.

VRF was found to have a significant influence on ENSO variability from 850 to 1850 (Le, 2017; Zuo et al., 2018) and robust relationship may thus exist between the ENSO and IOD (e.g. Cai et al., 2011; Le & Bae, 2019). Hence, the IOD's responses may be mediated by ENSO processes, and the models' capacities to simulate the ENSO-IOD relationship may create discrepancies in the causal effects of VRF on the IOD.

There are several reasons for the diversity in the response of tropical Indian Ocean to external forcings. For example, previous studies mentioned the spread in the model simulations related to thermocline feedback in the tropical Indian Ocean

(Zheng et al., 2013) and the amplitude of the IOD (Chu et al., 2014; Weller and Cai, 2013). In fact, the model biases related to the amplitude of the IOD still persist in CMIP6 models (McKenna et al., 2020). In addition, there is also inconsistency in the use of climate forcing inputs for different models as described in Supplemental Table S1. Besides, the biases in modeling the influence of the tropical Pacific on the tropical Indian Ocean might also cause the diversity in IOD response to external forcings.

Summary and conclusion

In this study, a Granger causality test was used to evaluate the influence of external forcings on the Indian Ocean Dipole (IOD) based on past millennium (past 1000) simulations of Coupled Model Intercomparison Project Phase 5 (CMIP5) models. Ten different models were applied to a causal analysis assessing the impact of external forcings on the IOD. Reconstructions of the IOD for the past 1000 years are still poorly constrained (e.g. Abram et al., 2015; Tierney et al., 2015). Thus, climate model simulations allow us to evaluate responses of the IOD to external forcings.

The results show that IOD variations of the past 1000 years were likely to exhibit weak responses to GHG radiative and solar forcing. Specifically, the probability of there being no Granger causality between GHG radiative forcing (or TSI) and the DMI is higher than 50% according to most models (see Figures 3 and 5). However, the results of this study only focus on pre-industrial times of the past 1000 years and may not hold for industrial periods or for the future and especially in terms of the possible effects of changes in GHGs on the IOD. The impact of volcanic forcing on the IOD is not entirely clear from the examined models. Four models (MPI-ESM-P, MRI-CGCM3, GISS-E2-R and CCSM4) show a significant causal influence of VRF on the IOD while other models show no significant impact. A further analysis of the four models shows a significant causal influence of volcanic forcing on Indian Ocean (IO) boreal autumn SST while responses of IO zonal winds to VRF are not significant. Thus, changes in IO zonal winds following volcanic eruptions may not directly contribute to the causal influence of VRF on IO SST and the IOD. The phase response (i.e. positive or negative) of the IOD to large volcanic eruptions remains unclear even for models showing a significant connection between VRF and the IOD. This result suggests that the IOD has a more complex response to volcanic forcing than the ENSO.

Uncertainties that may affect the IOD's responses to volcanic forcing and the potential influence of solar forcing on the IOD at the decadal and centennial timescales highlight the need to better understand the IOD's responses to external forcings. The results presented here may be further examined through additional model simulations of longer time periods, especially in terms of the linkages between volcanic forcing and the IOD. The fourth phase of the Paleoclimate Model Intercomparison Project (PMIP4) (Jungclaus et al., 2017) and the Model Intercomparison Project on the climatic response to Volcanic forcing (VolMIP) (Zanchettin et al., 2016) will serve as important efforts for evaluating the differences between model simulations and for improving our understanding of the influence of external forcings on the IOD. Besides, using Earth system Models of Intermediate Complexity (EMICs) forced by different external forcings is an approach to examine the sensitivity of the responses of the IOD. In addition, the use of other statistical methods (e.g. the bootstrap test) are necessary to evaluate the influences of external forcings on the IOD. The causal connection between the ENSO and IOD for the past 1000 years may be a topic of future research. Additional information on the ENSO-IOD causal relationship may improve our understanding of the influence of volcanic forcing on the IOD.

ORCID iD

Thanh Le (iD) https://orcid.org/0000-0001-5809-2751

Supplemental material

Supplemental material for this article is available online.

References

Abram NJ, Dixon BC, Rosevear MG et al. (2015) Optimized coral reconstructions of the Indian Ocean Dipole: An assessment of location and length considerations. *Paleoceanography* 30(10): 1391–1405.

Abram NJ, Gagan MK, McCulloch MT et al. (2003) Coral reef death during the 1997 Indian Ocean Dipole linked to Indonesian wildfires. *Science* 301(5635): 952–955.

Ashok K, Guan Z and Yamagata T (2003) Influence of the Indian Ocean Dipole on the Australian winter rainfall. *Geophysical Research Letters* 30(15): 3–6.

Behera SK, Luo JJ, Masson S et al. (2006) Paramount impact of the Indian ocean dipole on the East African short rains: A CGCM study. *Journal of Climate* 19(7): 1361.

Black E, Slingo JM and Sperber KR (2003) An observational study of the relationship between excessively strong short rains in coastal East Africa and Indian Ocean SST. *Monthly Weather Review* 131: 74–94.

Cai W, Cowan T and Sullivan A (2009) Recent unprecedented skewness towards positive Indian Ocean Dipole occurrences and its impact on Australian rainfall. *Geophysical Research Letters* 36(11): 1–4.

Cai W, Santoso A, Wang G et al. (2014) Increased frequency of extreme Indian Ocean Dipole events due to greenhouse warming. *Nature* 510(7504): 254–258.

Cai W, Sullivan A and Cowan T (2011) Interactions of ENSO, the IOD, and the SAM in CMIP3 models. *Journal of Climate* 24(6): 1688–1704.

Cai W, Wu L, Lengaigne M et al. (2019) Pantropical climate interactions. *Science* 363(6430): eaav4236.

Cai W, Zheng X-T, Weller E et al. (2013) Projected response of the Indian Ocean Dipole to greenhouse warming. *Nature Geoscience* 6(12): 999–1007.

Chu JE, Ha KJ, Lee JY et al (2014) Future change of the Indian Ocean basin-wide and dipole modes in the CMIP5. *Climate Dynamics* 43(1–2): 535–551.

Crowley T, Zielinski G and Vinther B (2008) Volcanism and the little ice age. *PAGES News* 16(2): 22–23.

Delaygue G and Bard E (2010) An Antarctic view of Beryllium-10 and solar activity for the past millennium. *Climate Dynamics* 36(11–12): 2201–2218.

Ding Y and Carton J (2014) Ocean response to volcanic eruptions in Coupled Model Intercomparison Project 5 simulations. *Journal of Geophysical Research: Oceans* 119(9): 5622–5637.

Gao C, Robock A and Ammann C (2008) Volcanic forcing of climate over the past 1500 years: An improved ice core-based index for climate models. *Journal of Geophysical Research* 113(D23): D23111.

Gómez-Navarro JJ, Bothe O, Wagner S et al. (2015) A regional climate palaeosimulation for Europe in the period 1501-1990. Part II: Comparison with gridded reconstructions. *Climate of the Past* 11: 1077–1095.

Granger C (1969) Investigating causal relations by econometric models and cross-spectral methods. *Econometrica: Journal of the Econometric Society* 37(3): 424–438.

Hegerl GC, Hoegh-Guldberg O, Casassa G et al. (2010) Good practice guidance paper on detection and attribution related to anthropogenic climate change. In: Stocker TF, Field CB, Qin D et al. (eds) *Meeting Report of the Intergovernmental Panel on Climate Change Expert Meeting on Detection and Attribution of Anthropogenic Climate Change*: 1–8. Bern, Switzerland: IPCC Working Group I Technical Support Unit, University of Bern. Available at: https://wg1.ipcc.ch/docs/IPCC_D&A_GoodPracticeGuidancePaper-1.pdf

Izumo T, Khodri M, Lengaigne M et al. (2018) A subsurface Indian Ocean Dipole response to tropical volcanic eruptions. *Geophysical Research Letters* 45(17): 9150–9159.

Jungclaus JH, Bard E, Baroni M et al. (2017) Supplement of The PMIP4 contribution to CMIP6 – Part 3: The last millennium, scientific objective, and experimental design for the PMIP4 *past1000* simulations. *Geoscientific Model Development* 10(11): 4005–4033.

Khodri M, Izumo T, Vialard J et al. (2017) Tropical explosive volcanic eruptions can trigger El Niño by cooling tropical Africa. *Nature Communications* 8(1): 1–12.

Kripalani RH, Oh JH and Chaudhari HS (2009) Delayed influence of the Indian Ocean Dipole mode on the East Asia-West Pacific monsoon: Possible mechanism. *International Journal of Climatology* 30(2): 197–209.

Latif M and Barnett TP (1994) Interactions of the Tropical Oceans. *Journal of Climate* 8(4): 952–964.

Lazenby MJ, Todd MC, Chadwick R et al. (2018) Future precipitation projections over central and Southern Africa and the adjacent Indian Ocean: What causes the changes and the uncertainty? *Journal of Climate* 31(12): 4807–4826.

Le T (2015) Solar forcing of Earth's surface temperature in PMIP3 simulations of the last millennium. *Atmospheric Science Letters* 16(3): 285–290.

Le T (2017) ENSO response to external forcing in CMIP5 simulations of the last millennium. *Global and Planetary Change* 148: 105–112.

Le T and Bae D-H (2019) Causal links on Interannual Timescale between ENSO and the IOD in CMIP5 future simulations. *Geophysical Research Letters* 46(5): 2820–2828.

Le T, Sjolte J and Muscheler R (2016) The influence of external forcing on subdecadal variability of regional surface temperature in CMIP5 simulations of the last millennium. *Journal of Geophysical Research: Atmospheres* 121(4): 1671–1682.

Ljungqvist FC, Zhang Q, Brattström G et al. (2019) Centennial-Scale temperature change in last millennium simulations and proxy-based reconstructions. *Journal of Climate* 32(9): 2441–2482.

Lütkepohl H (1982) Non-causality due to omitted variables. *Journal of Econometrics* 19: 367–378.

Maher N, Mcgregor S, England MH et al. (2015) Effects of volcanism on tropical variability. *Geophysical Research Letters* 42(14): 6024–6033.

Meehl GA, Arblaster JM, Branstator G et al. (2008) A coupled Air–Sea response mechanism to solar forcing in the Pacific region. *Journal of Climate* 21(12): 2883–2897.

Mignot J, Khodri M, Frankignoul C et al. (2011) Volcanic impact on the Atlantic Ocean over the last millennium. *Climate of the Past* 7(4): 1439–1455.

Mosedale TJ, Stephenson DB, Collins M et al (2006) Granger causality of coupled climate processes: Ocean feedback on the North Atlantic oscillation. *Journal of Climate* 19(7): 1182–1194.

Ramaswamy V, Boucher O, Haigh DJ et al. (2001) Radiative forcing of climate change. In: Joos F and Srinivasan J (eds) *Climate Change 2001: The Scientific Basis. Contribution of Working Group I to the Third Assessment Report of the Intergovernmental Panel on Climate Change*: 351–416. Available at: https://www.ipcc.ch/site/assets/uploads/2018/03/TAR-06.pdf

Robock A (2000) Volcanic eruptions and climate. *Reviews of Geophysics* 38(2): 191–219.

Saji NH, Vinayachandran PN and Yamagata T (1999) A dipole in the tropical Indian Ocean. *Nature* 401(September): 360–363.

Schmidt GA, Jungclaus JH, Ammann CM et al. (2011) Climate forcing reconstructions for use in PMIP simulations of the last millennium (v1.0). *Geoscientific Model Development* 4(1): 33–45.

Schmidt GA, Jungclaus JH, Ammann CM et al. (2012) Climate forcing reconstructions for use in PMIP simulations of the Last Millennium (v1.1). *Geoscientific Model Development* 5(1): 185–191.

Schurer AP, Tett SFB and Hegerl GC (2013) Small influence of solar variability on climate over the past millennium. *Nature Geoscience* 7: 104–108.

Solanki SK, Krivova NA and Haigh JD (2013) Solar irradiance variability and climate. *Annual Review of Astronomy and Astrophysics* 51(1): 311–351.

Sprintall J, Gordon AL, Koch-Larrouy A et al. (2014) The Indonesian seas and their role in the coupled ocean-climate system. *Nature Geoscience* 7(7): 487–492.

Steinhilber F, Beer J and Fröhlich C (2009) Total solar irradiance during the Holocene. *Geophysical Research Letters* 36(19): L19704.

Stern DI and Kaufmann RK (2013) Anthropogenic and natural causes of climate change. *Climatic Change* 122(1–2): 257–269.

Swingedouw D, Mignot J, Ortega P et al. (2017) Impact of explosive volcanic eruptions on the main climate variability modes. *Global and Planetary Change* 150: 24–45.

Tangunan D, Baumann KH, Pätzold J et al. (2017) Insolation forcing of coccolithophore productivity in the western tropical Indian Ocean over the last two glacial-interglacial cycles. *Paleoceanography* 32(7): 692–709.

Taylor KE, Stouffer RJ and Meehl GA (2012) An overview of CMIP5 and the experiment design. *Bulletin of the American Meteorological Society* 93(4): 485–498.

Tierney JE, Abram NJ, Anchukaitis KJ et al. (2015) Tropical Corals 400 yrs reconstructed from coral archives. *Paleoceanography* 30(October): 226–252.

Tokinaga H, Xie SP, Deser C et al. (2012) Slowdown of the Walker circulation driven by tropical Indo-Pacific warming. *Nature* 491(7424): 439–443.

Ummenhofer CC, England MH, McIntosh PC et al. (2009) What causes southeast Australia's worst droughts? *Geophysical Research Letters* 36(4): L04706.

Vieira LEA, Solanki SK, Krivova NA et al. (2011) Evolution of the solar irradiance during the Holocene. *Astronomy & Astrophysics* 531: A6.

Wang Y, Lean J and Jr NS (2005) Modeling the Sun's magnetic field and irradiance since 1713. *The Astrophysical Journal* 625(1): 522–538.

Webster PJ, Moore a M, Loschnigg JP et al. (1999) Coupled ocean-atmosphere dynamics in the Indian Ocean during 1997-98. *Nature* 401(6751): 356–360.

Weller E and Cai W (2013) Realism of the indian ocean dipole in CMIP5 models: The implications for climate projections. *Journal of Climate* 26(17): 6649–6659.

Zambri B, LeGrande AN, Robock A et al. (2017) Northern Hemisphere winter warming and summer monsoon reduction after volcanic eruptions over the last millennium. *Journal of Geophysical Research Atmospheres* 122(15): 7971–7989.

Zanchettin D, Khodri M, Timmreck C et al. (2016) The Model Intercomparison Project on the climatic response to Volcanic forcing (VolMIP): Experimental design and forcing input data. *Geoscientific Model Development* 9(8): 2701–2719.

Zheng X-T, Xie S-P, Du Y et al. (2013) Indian Ocean Dipole Response to Global Warming in the CMIP5 Multimodel Ensemble*. *Journal of Climate* 26(16): 6067–6080.

Zuo M, Man W, Zhou T et al. (2018) Different impacts of Northern, Tropical, and Southern volcanic eruptions on the tropical Pacific SST in the last millennium. *Journal of Climate* 31(17): 6729–6744.